

Transport coefficients for the hot quark-gluon plasma at finite chemical potential μ_B

Olga Soloveva*

Institute for Theoretical Physics, Johann Wolfgang Goethe-Universität, Frankfurt am Main, Germany

Pierre Moreau

*Department of Physics, Duke University, Durham, North Carolina 27708, USA,
Institute for Theoretical Physics, Johann Wolfgang Goethe-Universität, Frankfurt am Main, Germany*

Elena Bratkovskaya

*GSI Helmholtzzentrum für Schwerionenforschung GmbH, Darmstadt, Germany,
Institute for Theoretical Physics, Johann Wolfgang Goethe-Universität, Frankfurt am Main, Germany
(Dated: March 3, 2022)*

We calculate transport coefficients of the quark-gluon plasma (QGP) within the dynamical quasiparticle model (DQPM) by explicitly computing the parton interaction rates as a function of temperature T and baryon chemical potential μ_B on the basis of the DQPM couplings and partonic propagators. The latter are extracted from lattice QCD by matching the equation of state, entropy density and energy density at $\mu_B=0$. For baryon chemical potentials $0 \leq \mu_B \leq 500 \text{ MeV}$ we employ a scaling Ansatz for the effective coupling which was shown before to lead to thermodynamic consistent results in this range. We compute the ratio of the shear and bulk viscosities to the entropy density, i.e. η/s and ζ/s , the electric conductivity σ_0/T as well as the baryon diffusion coefficient κ_B and compare to related approaches from the literature. We find that the ratios η/s and ζ/s as well as σ_0/T are in accord with the results from lattice QCD at $\mu_B=0$ and only weakly depend on the ratio $T/T_c(\mu_B)$ where $T_c(\mu_B)$ denotes the critical temperature at finite baryon chemical potential.

I. INTRODUCTION

The exploration of the QCD phase diagram at non-zero baryon density (or baryon chemical potential) is the mission driving a number of actual and future heavy-ion collision (HIC) experiments. Whereas at ultra-relativistic energies at the Large Hadron Collider (LHC) or the Relativistic Heavy-Ion Collider (RHIC) the quark-gluon plasma, which is created in the central interaction volume, has almost zero baryon chemical potential ($\mu_B \approx 0$) and the transition from the deconfined state of quarks and gluons to the confined state of hadrons is a rapid but smooth crossover, the nature of the transition can not be understood from lattice QCD due to the fermionic sign problem at finite μ_B . Only for small chemical potentials an expansion in terms of higher order susceptibilities gives some orientation, but at higher μ_B one presently has to employ theoretical models. In order to reach the region of the QCD phase diagram at finite baryon chemical potentials ongoing experiments are decreasing the center-of-mass collision energy and measuring observables at mid-rapidity. So far, the Beam Energy Scan (BES) program at RHIC has carried out a series of Au+Au collisions with the range of $\sqrt{s_{NN}}$ starting from 200 GeV down to 7.7 GeV. According to the statistical models the corresponding baryon chemical potential at chemical freeze-out is varying from $\mu_B \approx 20 \text{ MeV}$ at $\sqrt{s_{NN}} = 200 \text{ GeV}$ to $\approx 420 \text{ MeV}$ at $\sqrt{s_{NN}} = 7.7 \text{ GeV}$ [1]. To study the existence of a critical end point (CEP)

and possible effects of a first-order phase transition a rising of the baryon chemical potential can be achieved by further lowering the collision energy in the proposed BES phase III of fixed-target experiments and also in the future experiments at FAIR (Facility for Antiproton and Ion Research) [2] and NICA (Nuclotron-based Ion Collider fAcility) [3] that particularly address the QGP phase diagram at moderate and higher μ_B .

Theoretical methods to explore QCD in Minkowski space for non-vanishing quark (or baryon) potentials are essentially effective approaches in which one can study the dominant properties of QCD in equilibrium, i.e. the thermodynamic quantities as well as transport coefficients. To this aim, the dynamical quasiparticle model (DQPM) has been introduced [4] which is based on partonic propagators with sizeable imaginary parts of the self-energies incorporated. Whereas the real part of the self-energies can be attributed to a dynamically generated mass (squared) of the partons the imaginary parts contain the information about the interaction rates in the system. Furthermore, the imaginary parts of the propagators define the spectral functions of the degrees of freedom which might show characteristic quasiparticle peaks. A further advantage of a propagator based approach is that one can formulate a consistent thermodynamics [5, 6] as well as a causal theory for non-equilibrium configurations on the basis of Kadanoff-Baym (KB) equations. Transport coefficients are particularly interesting since they reveal the information about the interactions in the medium which in equilibrium can be characterized by a temperature T and chemical potential μ_B . There are also a lot of alternative effective models describing the partonic phase of the heavy-ion collision. While ba-

* soloveva@fias.uni-frankfurt.de

sically all of the effective models have similar equations of state (EoS), which match well with available lattice data, the transport coefficients can vary significantly [7–9]. Moreover, an exploration of transport coefficients of the hot and dense QGP provides useful information for hydrodynamical simulations of HICs.

In this study we evaluate the T and μ_B dependence of transport coefficients for the strongly interacting QGP on the basis of microscopic collision rates that are evaluated from the effective coupling and propagators of the DQPM on the tree level following our earlier work in Ref. [10]. A related approach to transport coefficients has been recently presented in Ref. [11].

The paper is organized as follows: In Sec. II we give a brief review of the basic parton properties in the DQPM and describe the calculation of the equation of state including a specification of the different contributions to the entropy density. Sec. III is devoted to the actual computation of transport coefficients based on the relaxation time approximation, i.e. the shear and bulk viscosities, the electric conductivity as well as the baryon diffusion coefficient. We, furthermore, compare our results at $\mu_B = 0$ to calculations from lattice QCD for $N_f = 0$, predictions from a Bayesian analysis, and estimates based on the Chapman-Enskog method. We close our study with conclusions in Sec. IV.

II. PARTON PROPERTIES IN THE DQPM

In order to describe the partonic phase of heavy-ion collisions on the microscopic level, the dynamical quasiparticle model (DQPM) was introduced in Refs. [4, 12]. This effective model defines strongly-interacting quarks and gluons in terms of quasiparticles with single-particle (two-point) Greens functions in the form

$$G^R(\omega, \mathbf{p}) = \frac{1}{\omega^2 - \mathbf{p}^2 - M^2 + 2i\gamma\omega} \quad (1)$$

using $\omega = p_0$ for energy.

The coupling (squared) $g^2 = 4\pi\alpha_s$ regulates the strength of the interaction and enters the definition of the DQPM thermal masses and widths. Here we follow a procedure similar to Refs. [13, 14] to determine the effective coupling (squared) g^2 as a function of temperature T , i.e. the coupling is defined at $\mu_B = 0$ by a parametrization of the entropy density from lattice QCD in the following way:

$$g^2(s/s_{SB}) = d((s/s_{SB})^e - 1)^f, \quad (2)$$

with the Stefan-Boltzmann entropy density $s_{SB}^{QCD} = 19/9\pi^2 T^3$ and the parameters $d=169.934$, $e=-0.178434$ and $f=1.14631$. In the following, we use a parametrization of the entropy density at $\mu_B = 0$ calculated by lQCD from Refs. [15, 16] to determine the DQPM coupling g^2 as a function of temperature.

To obtain the coupling at finite baryon chemical potential μ_B , the scaling hypothesis assumes that g^2 is a function of the ratio of the effective temperature $T^* = \sqrt{T^2 + \mu_q^2/\pi^2}$ and the μ_B -dependent critical temperature $T_c(\mu_B)$ as:

$$g^2(T/T_c, \mu_B) = g^2\left(\frac{T^*}{T_c(\mu_B)}, \mu_B = 0\right), \quad (3)$$

with $\mu_B = 3\mu_q$, $T_c(\mu_B) = T_c\sqrt{1 - \alpha\mu_B^2}$, where T_c is the critical temperature at vanishing chemical potential (≈ 0.158 GeV) and $\alpha = 0.974$ GeV $^{-2}$ as in Ref. [10]. It was shown in Ref. [17] that this scaling Ansatz provides results for the partonic pressure P and quark density n_q that are practically equivalent to results from an integration of the Maxwell relations, that guarantee thermodynamic consistency for baryon chemical potentials less than 0.5 GeV. Thus, we limit our study to this range in μ_B , which accordingly to the statistical model roughly correspond to the averaged μ_B probed in nucleus-nucleus collisions at $\sqrt{s_{NN}} \approx 5$ GeV [18]. We mention that at even lower bombarding energies (and higher μ_B) the heavy-ion collisions dynamics was found to be dominated by hadronic degrees of freedom [19] with a low sensitivity to the partonic phase in small space-time volumes.

With the coupling g^2 fixed from lQCD one can now specify the masses of the dynamical quasiparticles, which are assumed to be given by the HTL thermal masses in the asymptotic high-momentum regime, i.e. for gluons by

$$M_g^2(T, \mu_B) = \frac{g^2(T, \mu_B)}{6} \left(\left(N_c + \frac{1}{2}N_f \right) T^2 + \frac{N_c}{2} \sum_q \frac{\mu_q^2}{\pi^2} \right), \quad (4)$$

and for quarks (antiquarks) by

$$M_{q(\bar{q})}^2(T, \mu_B) = \frac{N_c^2 - 1}{8N_c} g^2(T, \mu_B) \left(T^2 + \frac{\mu_q^2}{\pi^2} \right), \quad (5)$$

where $N_c = 3$ stands for the number of colors while $N_f (= 3)$ denotes the number of (light) flavors. The dynamical masses (5) in the QGP are large compared to the bare masses of the light (u, d) quarks and adopted in the form (5) for the (u, d) quarks. The strange quark has a larger bare mass which also enters to some extent the dynamical mass $M_s(T)$. This essentially suppresses the channel $g \rightarrow s + \bar{s}$ relative to the channel $g \rightarrow u + \bar{u}$ or $d + \bar{d}$ and controls the strangeness ratio in the QGP. Empirically $M_s(T, \mu_B) = M_u(T, \mu_B) + \Delta M = M_d(T, \mu_B) + \Delta M$ where $\Delta M = 30$ MeV has been used. This parameter has been fixed once in comparison to experimental data for the K^+/π^+ ratio in central Au+Au collisions at $\sqrt{s_{NN}} = 200$ GeV. Furthermore, the quasiparticles in the DQPM have finite widths, which are adopted in the form [12]

$$\gamma_g(T, \mu_B) = \frac{1}{3} N_c \frac{g^2(T, \mu_B) T}{8\pi} \ln \left(\frac{2c}{g^2(T, \mu_B)} + 1 \right), \quad (6)$$

$$\gamma_{q(\bar{q})}(T, \mu_B) = \frac{1}{3} \frac{N_c^2 - 1}{2N_c} \frac{g^2(T, \mu_B) T}{8\pi} \ln \left(\frac{2c}{g^2(T, \mu_B)} + 1 \right), \quad (7)$$

where $c = 14.4$ is related to a magnetic cut-off, which is an additional parameter of the DQPM. Furthermore, we assume that the width of the strange quark is the same as that for the light (u, d) quarks. At large temperatures the masses and widths grow linearly with the temperature whereas at temperatures close to $T_c(\mu_B)$ the DQPM masses are enhanced. Furthermore, the behavior at finite baryon chemical potential follows the one of the coupling $g^2(T, \mu_B)$ and thus a decrease is observed with increasing μ_B . We mention that the finite width of the propagator γ_i (6), (7) is related to the collision rate of parton $i = q(\bar{q}), g$ by $\Gamma_i = 2\gamma_i$. In this way we can check if the parametrizations (6), (7) are consistent with the collisional widths computed microscopically (see below).

With the quasiparticle properties (or propagators) fixed as described above, one can evaluate the entropy density $s(T, \mu_B)$, the pressure $P(T, \mu_B)$ and energy density $\epsilon(T, \mu_B)$ in a straight forward manner by starting with the entropy density and number density in the propagator representation from Baym [5, 6],

$$s^{dqp} = \quad (8)$$

$$\begin{aligned} & - \int \frac{d\omega}{2\pi} \frac{d^3p}{(2\pi)^3} \left[d_g \frac{\partial n_B}{\partial T} (\text{Im}(\ln -\Delta^{-1}) + \text{Im} \Pi \text{Re} \Delta) \right. \\ & + \sum_{q=u,d,s} d_q \frac{\partial n_F(\omega - \mu_q)}{\partial T} (\text{Im}(\ln -S_q^{-1}) + \text{Im} \Sigma_q \text{Re} S_q) \\ & \left. + \sum_{\bar{q}=\bar{u},\bar{d},\bar{s}} d_{\bar{q}} \frac{\partial n_F(\omega + \mu_q)}{\partial T} (\text{Im}(\ln -S_{\bar{q}}^{-1}) + \text{Im} \Sigma_{\bar{q}} \text{Re} S_{\bar{q}}) \right] \end{aligned}$$

$$n^{dqp} = - \int \frac{d\omega}{2\pi} \frac{d^3p}{(2\pi)^3} \quad (9)$$

$$\begin{aligned} & \left[\sum_{q=u,d,s} d_q \frac{\partial n_F(\omega - \mu_q)}{\partial \mu_q} (\text{Im}(\ln -S_q^{-1}) + \text{Im} \Sigma_q \text{Re} S_q) \right. \\ & \left. + \sum_{\bar{q}=\bar{u},\bar{d},\bar{s}} d_{\bar{q}} \frac{\partial n_F(\omega + \mu_q)}{\partial \mu_q} (\text{Im}(\ln -S_{\bar{q}}^{-1}) + \text{Im} \Sigma_{\bar{q}} \text{Re} S_{\bar{q}}) \right], \end{aligned}$$

where $n_B(\omega) = (\exp(\omega/T) - 1)^{-1}$ and $n_F(\omega - \mu_q) = (\exp((\omega - \mu_q)/T) + 1)^{-1}$ denote the Bose-Einstein and Fermi-Dirac distribution functions, respectively, while $\Delta = (p^2 - \Pi)^{-1}$, $S_q = (p^2 - \Sigma_q)^{-1}$ and $S_{\bar{q}} = (p^2 - \Sigma_{\bar{q}})^{-1}$ stand for the full (scalar) quasiparticle propagators of gluons g , quarks q and antiquarks \bar{q} . In Eq. (8)-(9)

Π and $\Sigma = \Sigma_q \approx \Sigma_{\bar{q}}$ denote the (retarded) quasiparticle self-energies. Furthermore, the number of transverse gluonic degrees-of-freedom is $d_g = 2 \times (N_c^2 - 1)$ while for the fermion degrees-of-freedom we use $d_q = 2 \times N_c$ and $d_{\bar{q}} = 2 \times N_c$.

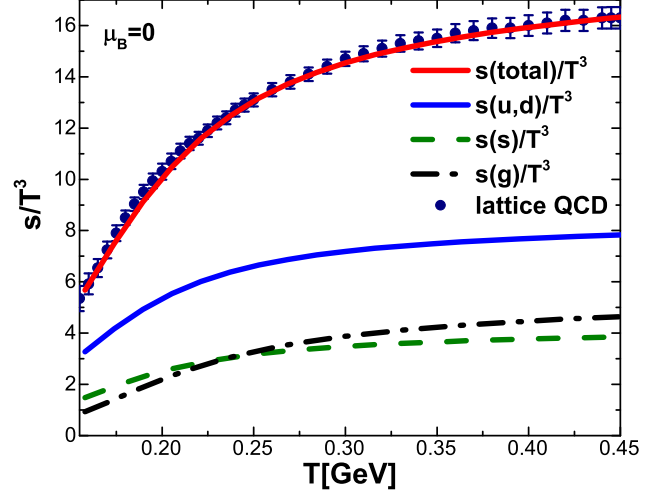


FIG. 1. The scaled entropy density $s(T)/T^3$ from the DQPM for different quasiparticle species: light quarks (solid blue line), stange quarks (dot-dashed green line), gluons (dashed black line), total (red line) in comparison to the IQCD results from Ref. [16] (full dots) for $\mu_B = 0$.

In principle, Π as well as Δ are Lorentz tensors and should be evaluated in a nonperturbative framework. The DQPM treats these degrees-of-freedom as independent scalar fields (for each color and spin projection) with scalar self-energies which are assumed to be identical for quarks and antiquarks. This is expected to hold well for the entropy and number density. Note that at finite quark chemical potential $\mu_q = \mu_B/3$ one has to deal with quarks and antiquarks separately in Eqs. (8)-(9) since their abundance differs.

In case the real and imaginary parts of the propagators Δ and S are fixed, the entropy density (8) and number density (9) can be evaluated numerically. As we deal with a grand-canonical ensemble, where the negative pressure is the thermodynamic potential, the Maxwell relations give

$$s = \frac{\partial P}{\partial T} \quad ; \quad n_B = \frac{\partial P}{\partial \mu_B}, \quad (10)$$

such that the pressure P (and thus the thermodynamic potential) can be obtained by integration of the entropy density s over T and of the baryon density n_B over μ_B as:

$$P(T, \mu_B) = P(T_0, 0) \quad (11)$$

$$+ \int_{T_0}^T s(T', 0) dT' + \int_0^{\mu_B} n_B(T, \mu'_B) d\mu'_B$$

where one identifies the 'full' entropy density s and baryon density n_B with the quasiparticle entropy density s^{dqp} (8) and baryon density $n_B = n^{dqp}/3$ (9). The starting point T_0 for the integration in T is chosen between $0.1 < T < 0.15$ GeV where the entropy density is taken in accordance to the lattice QCD results from Ref. [15] in the hadronic sector.

The energy density ϵ then follows from the thermodynamical relation

$$\epsilon = Ts - P + \mu_B n_B \quad (12)$$

and thus is also fixed by the entropy $s(T, \mu_B)$ and baryon density $n_B(T, \mu_B)$ as well as the interaction measure

$$I := \epsilon - 3P = Ts - 4P + \mu_B n_B \quad (13)$$

that vanishes for massless and noninteracting degrees of freedom at $\mu_B = 0$.

A good agreement between the resulting entropy density $s(T)$ (8), pressure $P(T)$ (11), energy density $\epsilon(T)$ (12) and interaction measure $I(T)$ (13) from the DQPM and the lQCD results obtained by the BMW group [15, 16] for $\mu_B = 0$ and $\mu_B = 400$ MeV has been shown in Ref. [10]. For completeness and transparency the resulting entropy densities for different quasiparticles are shown in Fig. 1, along with the lattice QCD results from Ref. [16]. The main contribution to the entropy density comes from the light quarks and antiquarks, while strange quarks have smaller contributions due to their larger mass. The contribution of gluons is of the same order, although these have an even larger mass and width, due to the degeneracy factor $d_g = 2(N_c^2 - 1) = 16$, which is larger than the strange quark degeneracy factor $d_s = 6$.

III. TRANSPORT COEFFICIENTS

In this section we calculate transport coefficients of the QGP in equilibrium within the DQPM thus extending our previous work in Ref. [10]. We will consider the shear η and bulk ζ viscosities, the electric conductivity σ_0 and the baryon diffusion coefficient κ_B . It has been found that in the quasi-particle approximation results for transport coefficients from the relaxation time approximation (RTA) of kinetic theory [20, 23–25] and from the one-loop diagram calculations based on Kubo relations [21, 22, 26, 27] are very close. All transport coefficients, which we will describe later on, have been calculated within the relaxation time approximation (RTA). The first step in the calculation of transport coefficients

within the RTA framework is the evaluation of relaxation times, which are supposed to depend on momenta, temperature, and baryon chemical potential. We have considered two cases for the relaxation times for quarks and gluons:

$$1) \tau_i(\mathbf{p}, T, \mu_B) = \frac{1}{\Gamma_i(\mathbf{p}, T, \mu_B)}$$

$$2) \tau_i(T, \mu_B) = \frac{1}{2\gamma_i(T, \mu_B)}, \quad (14)$$

where $\Gamma_i(\mathbf{p}, T, \mu_B)$ is the parton interaction rate based on the microscopic differential cross sections computed in Ref. [10], while $\gamma_i(T, \mu_B)$ are the parton spectral widths from (6), (7). For a detailed description of the differential partonic cross sections at finite T and μ_B on the level of tree diagrams we refer the reader to Ref. [10]. We briefly recall that in the on-shell case (energies of the particles are taken to be $E^2 = \mathbf{p}^2 + M^2$ where M is the pole mass) the collisional widths are calculated as follows:

$$\Gamma_i^{\text{on}}(\mathbf{p}_i, T, \mu_q) = \frac{1}{2E_i} \sum_{j=q, \bar{q}, g} \int \frac{d^3 p_j}{(2\pi)^3 2E_j} d_j f_j(E_j, T, \mu_q)$$

$$\times \int \frac{d^3 p_3}{(2\pi)^3 2E_3} \int \frac{d^3 p_4}{(2\pi)^3 2E_4} (1 \pm f_3)(1 \pm f_4)$$

$$\times |\bar{\mathcal{M}}|^2(p_i, p_j, p_3, p_4) (2\pi)^4 \delta^{(4)}(p_i + p_j - p_3 - p_4)$$

$$= \sum_{j=q, \bar{q}, g} \int \frac{d^3 p_j}{(2\pi)^3} d_j f_j v_{\text{rel}} \int d\sigma_{ij \rightarrow 34}^{\text{on}} (1 \pm f_3)(1 \pm f_4), \quad (15)$$

where d_j is the degeneracy factor for spin and color (for quarks $d_q = 2 \times N_c$ and for gluons $d_g = 2 \times (N_c^2 - 1)$), and with the shorthand notation $f_j = f_j(E_j, T, \mu_q)$ for the distribution functions. In Eq. (15) and in all this section, the notation $\sum_{j=q, \bar{q}, g}$ includes the contribution from all possible partons which in our case are the gluons and the (anti-)quarks of three different flavors (u, d, s). Furthermore, v_{rel} denotes the relative velocity of the colliding partons whereas $\sigma_{ij \rightarrow 34}^{\text{on}}$ stand for the differential cross sections computed in Ref. [10].

It is interesting to evaluate the parton relaxation times as a function of temperature T and chemical potential μ_B times. To this aim we calculate the average width of the partons i , we finally have to average its interaction rate (15) over its momentum distribution,

$$\Gamma_i^{\text{on}}(T, \mu_q) = \frac{d_i}{n_i^{\text{on}}(T, \mu_q)} \int \frac{d^3 p_i}{(2\pi)^3} f_i(E_i, T, \mu_q)$$

$$\times \Gamma_i^{\text{on}}(\mathbf{p}_i, T, \mu_q) \quad (16)$$

with the on-shell density of partons i at T and μ_q given by

$$n_i^{\text{on}}(T, \mu_q) = d_i \int \frac{d^3 p_i}{(2\pi)^3} f_i(E_i, T, \mu_q). \quad (17)$$

In fact, as seen from Eq. (15), the interaction rate of particle i is directly proportional to the density of the colliding partner j and its degeneracy factor d_j , and to their interaction cross section σ_{ij} as:

$$\Gamma_i \propto \sum_j d_j f_j \sigma_{ij}. \quad (18)$$

If we consider e.g. u -quark scattering, we obtain for all the possible interaction channels:

- (1) : $uu \rightarrow uu$; $\Gamma_{uu \rightarrow uu} \propto d_u f_u \sigma_{uu \rightarrow uu}$ (t + u channels)
- (2) : $u\bar{u} \rightarrow u\bar{u}$; $\Gamma_{u\bar{u} \rightarrow u\bar{u}} \propto d_{\bar{u}} f_{\bar{u}} \sigma_{u\bar{u} \rightarrow u\bar{u}}$ (t + s channels)
- (3) : $u\bar{u} \rightarrow d\bar{d}$; $\Gamma_{u\bar{u} \rightarrow d\bar{d}} \propto d_{\bar{u}} f_{\bar{u}} \sigma_{u\bar{u} \rightarrow d\bar{d}}$ (s channel)
- (4) : $u\bar{u} \rightarrow s\bar{s}$; $\Gamma_{u\bar{u} \rightarrow s\bar{s}} \propto d_{\bar{u}} f_{\bar{u}} \sigma_{u\bar{u} \rightarrow s\bar{s}}$ (s channel)
- (5) : $ud \rightarrow ud$; $\Gamma_{ud \rightarrow ud} \propto d_d f_d \sigma_{ud \rightarrow ud}$ (t channel)
- (6) : $u\bar{d} \rightarrow u\bar{d}$; $\Gamma_{u\bar{d} \rightarrow u\bar{d}} \propto d_{\bar{d}} f_{\bar{d}} \sigma_{u\bar{d} \rightarrow u\bar{d}}$ (t channel)
- (7) : $us \rightarrow us$; $\Gamma_{us \rightarrow us} \propto d_s f_s \sigma_{us \rightarrow us}$ (t channel)
- (8) : $u\bar{s} \rightarrow u\bar{s}$; $\Gamma_{u\bar{s} \rightarrow u\bar{s}} \propto d_{\bar{s}} f_{\bar{s}} \sigma_{u\bar{s} \rightarrow u\bar{s}}$ (t channel)
- (9) : $ug \rightarrow ug$; $\Gamma_{ug \rightarrow ug} \propto d_g f_g \sigma_{ug \rightarrow ug}$ (t channel).

Adding up all the contributions, we get for the light quark total interaction rate:

$$\begin{aligned} \Gamma_u &= \sum_q \Gamma_{uq} + \sum_{\bar{q}} \Gamma_{u\bar{q}} + \Gamma_{ug} \\ &= (1) + (5) + (7) + (2) + (3) + (4) + (6) + (8) + (9). \end{aligned} \quad (19)$$

Similarly for a gluon g , the possible interaction channels are:

- (10) : $gu \rightarrow gu$; $\Gamma_{gu \rightarrow gu} \propto d_u f_u \sigma_{gu \rightarrow gu} = gd \rightarrow gd$; $\Gamma_{gd \rightarrow gd} \propto d_d f_d \sigma_{gd \rightarrow gd}$ (t + u + s channels)
- (11) : $g\bar{u} \rightarrow g\bar{u}$; $\Gamma_{g\bar{u} \rightarrow g\bar{u}} \propto d_{\bar{u}} f_{\bar{u}} \sigma_{g\bar{u} \rightarrow g\bar{u}} = g\bar{d} \rightarrow g\bar{d}$; $\Gamma_{g\bar{d} \rightarrow g\bar{d}} \propto d_{\bar{d}} f_{\bar{d}} \sigma_{g\bar{d} \rightarrow g\bar{d}}$ (t + u + s channels)
- (12) : $gs \rightarrow gs$; $\Gamma_{gs \rightarrow gs} \propto d_s f_s \sigma_{gs \rightarrow gs}$ (t + u + s channels)
- (13) : $g\bar{s} \rightarrow g\bar{s}$; $\Gamma_{g\bar{s} \rightarrow g\bar{s}} \propto d_{\bar{s}} f_{\bar{s}} \sigma_{g\bar{s} \rightarrow g\bar{s}}$ (t + u + s channels)
- (14) : $gg \rightarrow gg$; $\Gamma_{gg \rightarrow gg} \propto d_g f_g \sigma_{gg \rightarrow gg}$ (t + u + s channels + 4 point amplitude).

Adding up all the contributions, we get for the gluon total interaction rate:

$$\begin{aligned} \Gamma_g &= \sum_q \Gamma_{gq} + \sum_{\bar{q}} \Gamma_{g\bar{q}} + \Gamma_{gg} \\ &= 2 \times (10) + (12) + 2 \times (11) + (13) + (14). \end{aligned} \quad (20)$$

In Ref. [10] we have shown explicitly the quark and

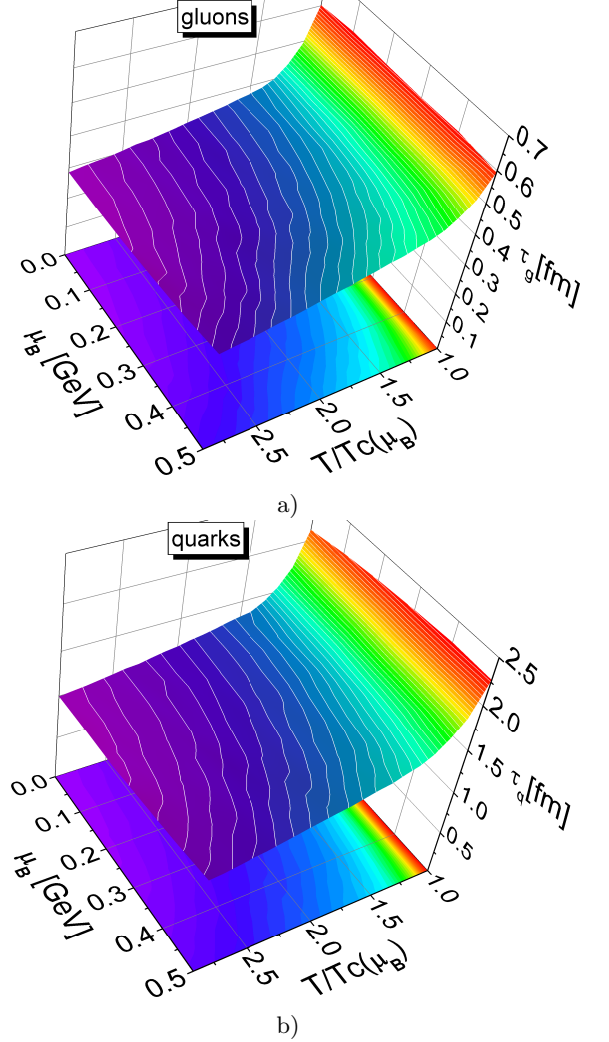


FIG. 2. Relaxation time of a gluon (a) and quark (b) as a function of the scaled temperature $T/T_c(\mu_B)$ and the baryon chemical potential μ_B evaluated by the average parton interaction rate from Eq. (16)

gluon off-shell interaction rates as a function of the scaled temperature $T/T_c(\mu_B)$ and chemical potential μ_B . While the dependencies on temperature are similar for fixed μ_B we see a general slight decrease in the total widths with μ_B for fixed temperature; the parton relaxation times - evaluated by Γ_i^{-1} - then slightly increase with μ_B . Fig. 2 gives an overview of the relaxation time of a gluon (a) and quark (b) as a function of the scaled

temperature $T/T_c(\mu_B)$ and chemical potential μ_B . The gluon relaxation time is about $0.3 - 0.4$ fm/c in the region $1.5T_c \leq T \leq 3T_c$, which is significantly smaller than the quark relaxation time, which is about $1.0 - 1.5$ fm/c. Since the transport coefficients are directly proportional to the relaxation times, it is clear that the main contribution to the transport coefficients in the RTA stems from quarks and antiquarks.

A. Shear viscosity

The shear viscosity to entropy density ratio η/s for the QGP - created in the central region of high-energy heavy-ion collisions at Super Proton Synchrotron (SPS) and Relativistic Heavy-Ion Collider (RHIC) - was predicted to be very low [29–31]. While the ratio η/s is expected to be small the shear viscosity η as well as the entropy s of partonic system are high and scale with the temperature as $\propto T^3$ as shown in Fig. 1 and Fig. 3.

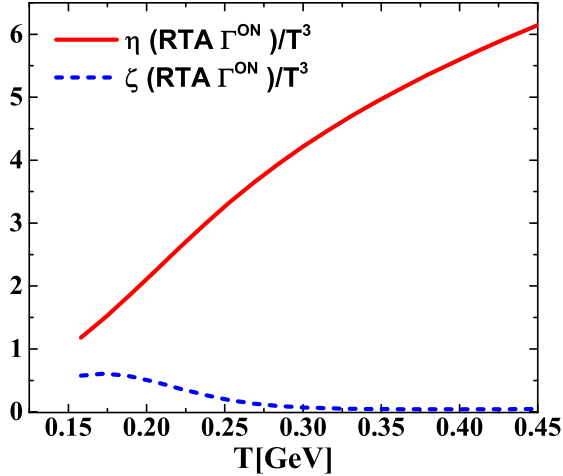


FIG. 3. Ratio of shear η/T^3 and bulk ζ/T^3 viscosities to the temperature cubed as a function of temperature for $\mu_B = 0$. The solid red line and the dashed blue line show the DQPM results for the shear and bulk ratios accordingly, using the parton interaction rate $\Gamma_i(\mathbf{p}, T, \mu)$ for the relaxation time.

One way to evaluate the viscosity coefficients of partonic matter is the Kubo formalism [21, 22, 26, 27], which was used to calculate the viscosities for a previous version of the DQPM within the PHSD transport approach in a box with periodic boundary conditions (cf. Ref. [28]). We here focus on the calculation of the shear viscosity based on the RTA [24] which reads:

$$\eta^{\text{RTA}}(T, \mu_B) = \frac{1}{15T} \sum_{i=q,\bar{q},g} \int \frac{d^3p}{(2\pi)^3} \frac{\mathbf{p}^4}{E_i^2} \tau_i(\mathbf{p}, T, \mu_B) \times d_i(1 \pm f_i)f_i, \quad (21)$$

where $d_q = 2N_c = 6$ and $d_g = 2(N_c^2 - 1) = 16$ are degeneracy factors for spin and color in case of quarks and gluons, τ_i are the relaxation times. In extension to our previous studies in Refs. [9, 13, 14] we here include the Pauli-blocking and Bose enhancement factors, respectively.

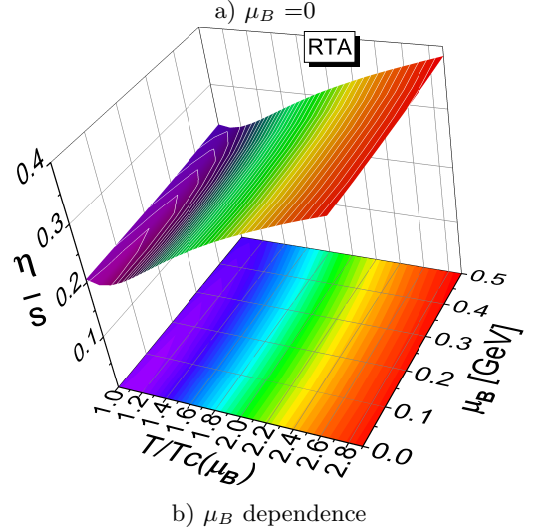
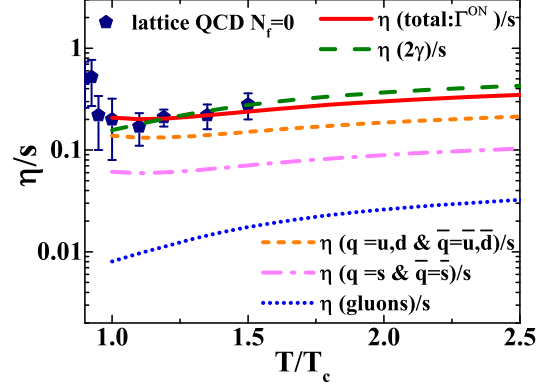


FIG. 4. Ratio of shear viscosity to entropy density a) as a function of scaled temperature T/T_c for $\mu_B = 0$ and b) for non-zero μ_B as a function of the scaled temperature $T/T_c(\mu_B)$ and the baryon chemical potential μ_B . The lines show the DQPM result from Eq. (21) using the interaction rate $\Gamma_i(\mathbf{p}, T, \mu)$ for different quasiparticle species: light quarks and anti-quarks (short dashed orange line), strange quarks and anti-quarks (dot-dashed magenta line), gluons (dotted blue line). The solid red line and the dashed green line show the DQPM results for total ratios of viscosity to entropy density using the parton interaction rate $\Gamma_i(\mathbf{p}, T, \mu)$ and the spectral width $2\gamma_i(T, \mu)$ for the relaxation time. The pentagons show the lQCD data for pure SU(3) gauge theory taken from Ref. [32].

The ratio of the shear viscosity to entropy density η/s has been presented before in Ref. [10]; it increases with an increase of the scaled temperature. The actual values for the ratio η/s are in a good agreement with the gluodynamic lattice QCD calculations at $\mu_B = 0$ from Ref. [32]. We find that the ratio η/s does not vary much

with μ_B and has a similar behavior as a function of temperature for all μ_B considered. The approximation (21) of the shear viscosity is found to be very close to the one from the Kubo formalism [10] indicating that the quasiparticle limit ($\gamma \ll M$) holds in the DQPM.

The ratio of the shear viscosity to entropy density at $\mu_B = 0$ is shown in Fig. 4 (a) in comparison to the lattice QCD calculation for $N_f = 0$ from Ref. [32]. The ratio η/s at $\mu_B = 0$ also is in a good agreement with the predictions from a Bayesian analysis of experimental heavy-ion data from Ref. [33]. In extension to Ref. [10] we also show the separate contributions to η/s for various quasiparticle species to the total ratio: light quarks and anti-quarks (short dashed orange line), strange quarks and anti-quarks (dot-dashed magenta line), gluons (dotted blue line). The solid red line correspond to the ratio of the total shear viscosity to entropy density. Smaller values of the shear viscosity are observed for the gluons than for the quarks as expected since the gluon relaxation time is approximately twice smaller than the quark relaxation time, and the masses of the gluons are approximately twice higher than quarks masses, which effects the shear viscosity via the factor $1/E_i^2$. The light quarks and anti-quarks give the main contribution to the total ratio $\sim 60\%$. The strange quarks and anti-quarks contribute by $\sim 30\%$, while the gluon contribution is about $\sim 10\%$. The differences for the shear viscosity of different quark flavour is essentially due to the mass difference. We mention that the hierarchy obtained here is in a good agreement with the recent calculations for the shear viscosity at $\mu_B = 0$ in the quasiparticle model of Ref. [11]. It is worth to note that in Ref. [11] only the on-shell case is considered where quasiparticles don't have widths and the couplings are higher than in the DQPM, which leads to an increase of the relaxation times and the shear viscosity to entropy density ratio η/s .

B. Bulk viscosity

The hydrodynamical simulations of ultrarelativistic heavy-ion collisions predicted that the bulk viscosity of the QGP should be non-zero, at least in the vicinity of the phase transition [34]. In this study we evaluate the bulk viscosity of the partonic phase within the RTA following Ref. [24]:

$$\zeta^{\text{RTA}}(T, \mu_B) = \frac{1}{9T} \sum_{i=q,\bar{q},g} \int \frac{d^3p}{(2\pi)^3} \tau_i(\mathbf{p}, T, \mu_B) \quad (22)$$

$$\times \frac{d_i(1 \pm f_i)f_i}{E_i^2} \left(\mathbf{p}^2 - 3c_s^2 \left(E_i^2 - T^2 \frac{dm_i^2}{dT^2} \right) \right)^2,$$

where c_s^2 is the speed of sound squared, $\frac{dm_i^2}{dT^2}$ is the DQPM parton mass derivative which becomes large close to the critical temperature T_c . The DQPM results for the viscosities over temperature cubed are showed at Fig. 3, where the parton interaction rate $\Gamma_i(\mathbf{p}, T, \mu_B)$ was used

for the relaxation time. The solid red line corresponds to the ratio of the shear viscosity to the temperature cubed η/T^3 , while the dashed blue line shows the ratio of bulk viscosity to the temperature cubed ζ/T^3 .

Fig. 5 a) shows the ratio of the bulk viscosity to entropy density ζ/s as a function of the scaled temperature T/T_c for $\mu_B = 0$. The solid red line ($\zeta_{\text{RTA}}^{\text{RTA}}/s$) displays the results from Eq. (22) using the interaction rate $\Gamma_i(\mathbf{p}, T, \mu)$ while the dashed green line shows the same result in the relaxation-time approximation (22) by replacing Γ_i by the spectral width $2\gamma_i$. The symbols correspond to the lQCD data for pure SU(3) gauge theory taken from Refs. [35](pentagons) and [36](circles). The solid blue line shows the results from a Bayesian analysis of experimental heavy-ion data from Ref. [37]. The bulk viscosities of our quasiparticle models are always smaller than the shear viscosities even close to the phase transition.

The DQPM results coincide with the lattice data, except the point at $T \approx T_c$ from Ref. [35]. This point has large error bars since lattice simulations at low temperatures require much larger statistics than simulations at higher T . We compare the bulk viscosity also to predictions from a Bayesian analysis of experimental data from Ref. [37]. The DQPM exhibits the expected peak close to the critical temperature which is close to the Bayesian line maximum of the peak at T_c with $\zeta/s \simeq 0.075$. The ratio from the Bayesian analysis shows a sudden drop to zero, which is incompatible with the small, non-zero lattice values. Furthermore, the DQPM results for viscosities are in a good agreement with the gluodynamic lattice QCD calculation at $\mu_B = 0$ from Ref. [35]. In the case of the bulk viscosity ζ we have found that the original DQPM calculations are very close to the results obtained using the interaction rates, such that they merge in Fig. 5 a). The ratio η/s increases with μ_B at all temperatures, while ζ/s only for $T > 1.2T_c$. It decreases in the vicinity of T_c , where the bulk viscosity is dominated by the mean-field effects that enter via dM^2/dT^2 . In the DQPM the masses depend primarily on the effective coupling g^2 , which decreases as a function of μ_B , also the mean-field effects become weaker. This causes a small decrease of ζ/s in contrast to the other transport coefficients. At higher temperatures the mean-field effects become also less pronounced, resulting in a decreasing ζ/s as a function of temperature. That clarifies why the μ_B behavior of the bulk viscosity changes with temperature. When the mean-field effects become subleading, their further decrease has no influence on the bulk viscosity and the ratio ζ/s starts to increase with μ_B as we will see later for the other transport coefficients.

C. Electric conductivity

Another important transport coefficient is the electric conductivity for stationary electric fields σ_0 which describes the response of the system to an external electric

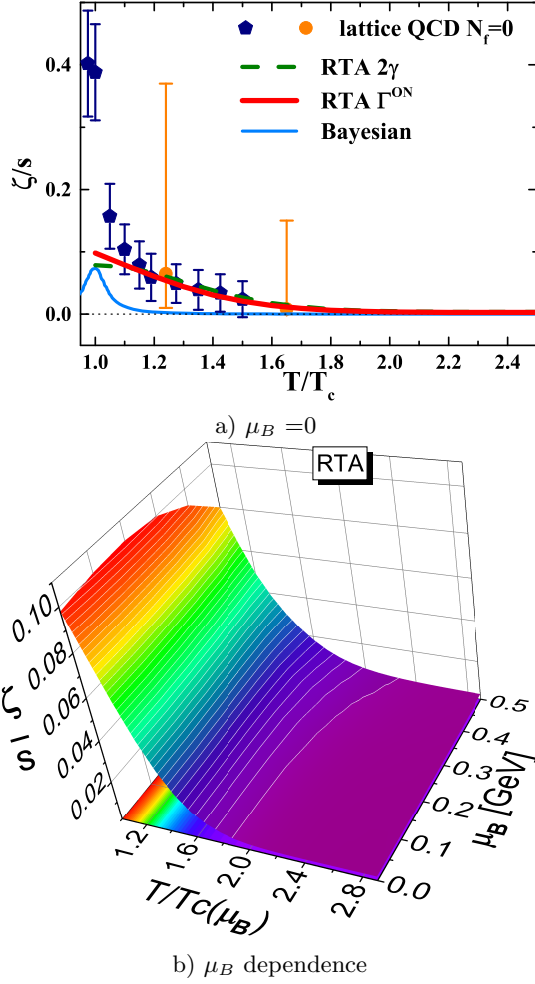


FIG. 5. Ratio of bulk viscosity to entropy density ζ/s a) as a function of scaled temperature T/T_c for $\mu_B = 0$ and b) for non-zero μ_B as a function of the scaled temperature $T/T_c(\mu_B)$ and the baryon chemical potential μ_B . The solid red line and the dashed green line show the DQPM results within the RTA from Eq. (22) using the parton interaction rate $\Gamma_i(\mathbf{p}, T, \mu)$ and the spectral width $2\gamma_i(T, \mu)$ for the relaxation time. The symbols display the IQCD data for $N_f = 0$ pure SU(3) gauge theory taken from Refs. [35] (pentagons) and [36] (circles). The solid blue line shows the estimate from a Bayesian analysis of experimental heavy-ion data taken from Ref. [37].

field. The study of the temperature and baryon chemical potential dependence of σ_0 is of fundamental importance for the possible generation of the chiral-magnetic effect in predominantly peripheral heavy-ion reactions. Moreover, σ_0 influences the emission rate of soft photons [40] as well as their spectra [41–43]. The electric conductivity σ_0 is evaluated by using the relaxation time approximation (see Ref. [45] for a detailed derivation):

$$\sigma_0^{\text{RTA}}(T, \mu_B) = \frac{e^2}{3T} \sum_{i=q,\bar{q}} q_i^2 \int \frac{d^3p}{(2\pi)^3} \frac{\mathbf{p}^2}{E_i^2} \times \tau_i(\mathbf{p}, T, \mu_B) d_i(1 - f_i)f_i, \quad (23)$$

where $e^2 = 4\pi\alpha_{em}$, $q_i = +2/3(u), -1/3(d), -1/3(s)$ are the quark charges, $d_q = 2N_c = 6$ are degeneracy factors for spin and color in case of quarks and anti-quarks, τ_i their relaxation times, while f_i denote the Fermi-Dirac distribution functions for quark and anti-quarks. In these formulae we deal with quarks and anti-quarks of $N_f = 3$ flavours. Each parton has a contribution proportional to its charge squared. Unlike viscosities, the electric conductivity doesn't contain a contribution from gluons.

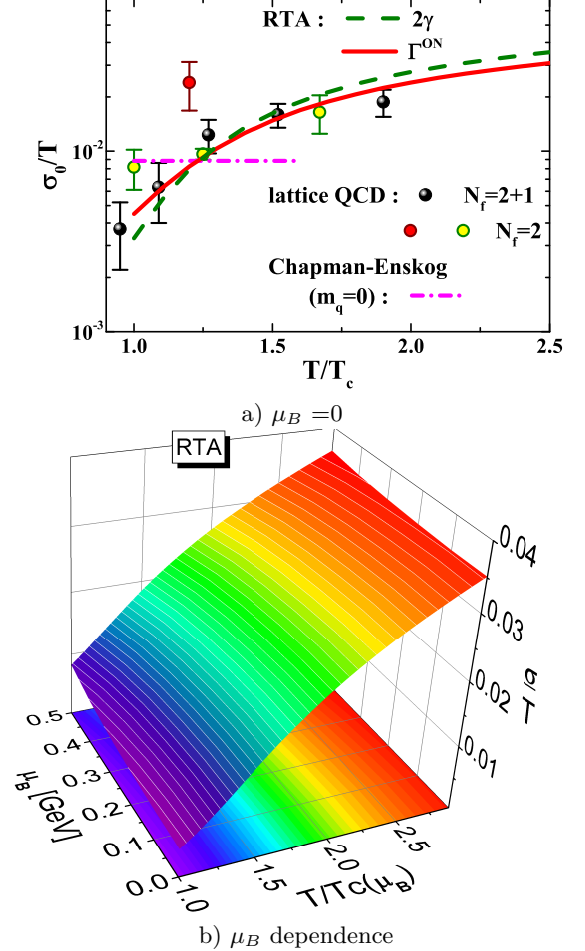


FIG. 6. Ratio of electric conductivity to temperature σ_0/T a) as a function of the scaled temperature T/T_c for $\mu_B = 0$ and b) for non-zero μ_B as a function of the scaled temperature $T/T_c(\mu_B)$ and the baryon chemical potential μ_B . The solid red line and the dashed green line show the DQPM results within the RTA from Eq. 23 using the parton interaction rate $\Gamma_i(\mathbf{p}, T, \mu)$ and the spectral width $2\gamma_i(T, \mu)$ for the relaxation time. The symbols display IQCD data for $N_f = 2$ taken from Refs. [46–48] (red circles with brown borders), (yellow circles with green borders) and for $N_f = 2 + 1$ taken from Refs. [49, 50] (spheres). The dot-dashed magenta line corresponds to the results from the first order Chapman-Enskog approximation taken from Ref. [51].

Fig. 6 depicts the results for σ_0/T a) as a function of the scaled temperature and b) the μ_B and T dependence from the DQPM. The solid red line shows the DQPM

result σ_0^{RTA}/T from Eq. (23) using the interaction rate $\Gamma_i(\mathbf{p}, T, \mu)$ while the dashed green line shows the result in the relaxation-time approximation (23) by replacing Γ_i by the spectral width $2\gamma_i(T, \mu)$. We find that both values for σ_0/T are in a good agreement. The differences between the two lines can vary by 14%, except close to T_c where the momentum dependencies of relaxation times can play a role. This approximate equivalence demonstrates again that the effective widths in the parton propagators - providing the spectral widths of the partons - are well in line with the microscopic collision rates. The ratio rises quadratically with temperature above T_c which is most likely due to the increasing number of quarks at higher temperatures. An increase in the number of charge carriers leads to an increasing electric current and therefore to an increasing conductivity. The momentum integration smoothes the temperature dependence of the ratio.

There is another way to compute the electric conductivity by solving the relativistic transport equations for partons in a box with periodic boundary conditions in the presence of an external electric field as in Refs. [39, 44]. We compare also to the estimate from the Chapman-Enskog method using cross-sections for massless quarks and gluons as in Ref. [51], which are fixed in order to describe the Kovtun-Son-Starinets bound for the shear viscosity to entropy density ratio $(\eta/s)_{KSS} = 1/(4\pi)$ [52], leading to $\sigma_{tot} \approx 0.72/T^2$. We find a good agreement in the vicinity of T_c . Furthermore, there are holographic calculations for σ_0/T [53], which are close to our results in the vicinity of the transition $T_c - 1.5T_c$, however, the temperature dependence of the ratio differs and the values at high temperatures are lower than the DQPM predictions.

D. Baryon diffusion

It is interesting to consider further transport coefficients which are expected to be more sensitive to the net baryon density of the system, e.g. the baryon diffusion coefficient. This transport coefficient reveals the response to inhomogeneities in the baryon density. The baryon diffusion coefficient regulates the dissipative part of the baryon current which can be expressed as :

$$\delta J_B^\mu = \kappa_B D^\mu \left(\frac{\mu_B}{T} \right), \quad (24)$$

where κ_B is the baryon diffusion coefficient, $D^\mu = d^\mu - u^\mu u^\nu d_\nu$ is the transverse gradient, while u^μ is the local fluid velocity. The dissipative baryon current can be related to the heat flow as $q^\mu = -\frac{\epsilon+p}{n_B} \delta J_B^\mu$ (see Refs [57],[56]) ,

$$q^\mu = \lambda \frac{n_B}{\epsilon+p} D^\mu \left(\frac{\mu_B}{T} \right), \quad (25)$$

where λ is the heat conductivity. Thus we can obtain a relation between the heat conductivity and the diffusion

coefficient:

$$\kappa_B = \lambda \left(\frac{n_B T}{\epsilon+p} \right)^2. \quad (26)$$

One can easily estimate that the values of these two coefficients differ by 2 orders of magnitude.

The diffusion coefficient can be calculated within the relaxation time approximation.

$$\begin{aligned} \kappa_B^{\text{RTA}}(T, \mu_B) &= \frac{1}{3} \sum_{i=q,\bar{q}} \int \frac{d^3 p}{(2\pi)^3} \mathbf{p}^4 \tau_i(\mathbf{p}, T, \mu_B) \\ &\times \frac{d_i(1 \pm f_i) f_i}{E_i^2} \left(b_a - \frac{n_B E_i}{\epsilon+p} \right)^2, \end{aligned} \quad (27)$$

where $b_i = \pm 1/3$ is the baryon number of quark and antiquark, n_B is the baryon density, $w = \epsilon + p$ is the enthalpy. Taking into account relation (26) one can see that Eq. (27) is in agreement with the RTA expression for the heat conductivity as derived in Ref. [24].

Fig. 7 shows the actual results for the baryon diffusion coefficient in the range of temperature and non-zero baryon chemical potential μ_B . We compare the DQPM results to the estimates based on the thermal conductivity results from the AdS/CFT correspondence [56]. Using the relation between the baryon diffusion coefficient and the heat conductivity (26), we can translate these results to the following expression:

$$\kappa_B^{SS} = 2\pi \frac{T s}{\mu_B^2} \left(\frac{n_B T}{\epsilon+p} \right)^2, \quad (28)$$

where s is the entropy density, n_B is the baryon density, $w = \epsilon + p$ is the enthalpy. We have calculated κ_B^{SS} using s , n_B , ϵ and p from the DQPM.

In the vicinity of T_c the DQPM values for the diffusion coefficient are in agreement with the calculations within the Chapman-Enskog first-order approximation using cross-sections for massless quarks and gluons in Ref. [51]. However, for higher temperatures the ratio $\kappa_B^{\text{RTA}}/T^2$ grows with temperature in the DQPM while the Chapman-Enskog results stay approximately constant $\kappa_B^{CE}/T^2 \sim 0.048$ for all temperatures. It is expected that κ_B has a more sizable μ_B -dependence than another transport coefficients and we see a slight decrease of the ratio $\kappa_B^{\text{RTA}}/T^2$ for the DQPM with increasing chemical potential μ_B , while results from other approaches $\kappa_B^{CE}/T^2 \sim 0.048$ and κ_B^{SS} are approximately μ_B independent for the considered region of μ_B . The same slight decrease has been seen in the holographic calculations in Ref. [53].

κ_B can be an interesting property of the partonic phase, which may have effects on observables: it has been found within the hybrid (hydrodynamics+transport transport) theoretical framework in Ref. [58] that the baryon diffusion enhances the difference between proton and antiproton mean transverse momenta and elliptic flow $v_2(p_T)$: decreases proton elliptic flow while increasing anti-proton elliptic flow. Further studies of elliptic

and direct flow within the extended parton-hadron-string dynamics (PHSD) transport approach can be made to quantify the effect. In the extended version of PHSD [10] the partonic sector is described by explicitly calculating the total and differential partonic scattering cross sections as a function of temperature T and baryon chemical potential μ_B on the basis of the effective propagators and couplings from the DQPM and thus is a suitable extension of the DQPM to nonequilibrium configurations as encountered in relativistic heavy-ion collisions.

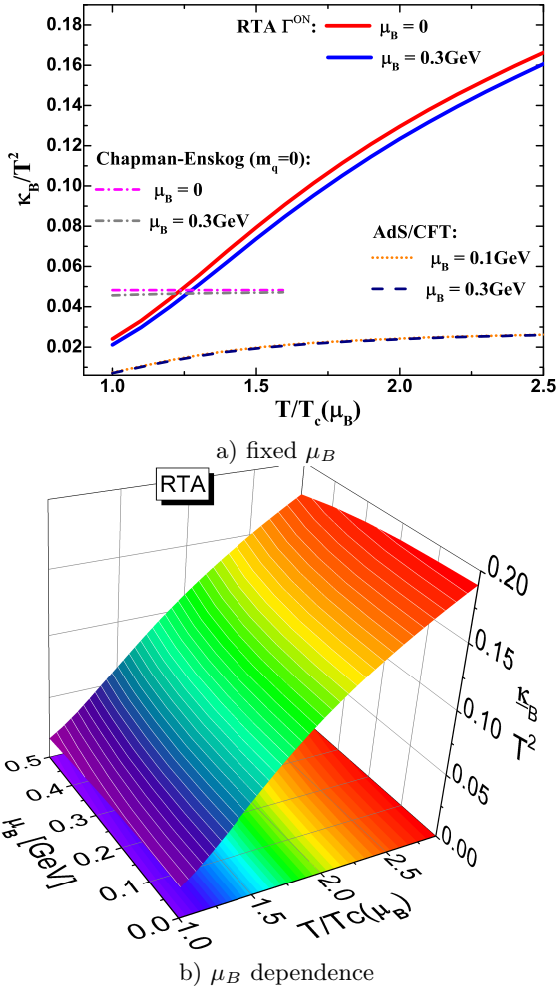


FIG. 7. Ratio of the baryon diffusion coefficient to the temperature squared κ_B/T^2 a) as a function of scaled temperature for fixed baryon chemical potential $\mu_B = 0$ and 0.3 GeV and b) as a function of scaled temperature for different values of the baryon chemical potential μ_B . The dashed lines represent the AdS/CFT results for κ_B^{SS} , which is obtained using the results from Ref. [56] and the DQPM EoS. The dot-dashed lines correspond to the results from the first order Chapman-Enskog approximation taken from Ref. [51].

IV. CONCLUSIONS

This study presents the results for transport coefficients of the QGP on the basis of the dynamical quasi-particle model DQPM. We have calculated the scaled temperature T/T_c and baryon chemical potential μ_B dependence of transport coefficients such as shear and bulk viscosity, electric conductivity and baryon diffusion coefficient. All calculations have been performed using the relaxation time approximation, where we have evaluated the relaxation times using a) the parton interaction rates $\tau_i(\mathbf{p}, T, \mu) = \frac{1}{\Gamma_i(\mathbf{p}, T, \mu)}$, where all the elastic two-body scatterings are employed, and b) the parton spectral widths $\tau_i(T, \mu) = \frac{1}{2\gamma_i(T, \mu)}$. The results for the transport coefficients - using two different evaluations of the relaxation time - are very close to each other and differ basically only close to the critical temperature.

In case of the shear viscosity η we showed the individual contributions of light quarks, strange quarks and gluons for $\mu_B=0$. The total ratio of the shear viscosity to entropy density η/s is in a good agreement with the most recent gluodynamic LQCD data and estimation from a Bayesian analysis of experimental data. This ratio grows smoothly with the baryon chemical potential for all temperatures in the considered range $\mu_B \leq 0.5$ GeV.

Furthermore, we have calculated the bulk viscosity to entropy density ratio ζ/s , which matches perfectly with the LQCD data at $\mu_B=0$, while the Bayesian analysis gives smaller values. The bulk viscosity has a (slight) μ_B dependence similar to the shear viscosity except in the vicinity of T_c , where mean-field effects play a role.

We have considered further transport coefficients such as the electric conductivity σ_0 and the baryon diffusion coefficient κ_B , where the gluons contribute only via the relaxation times. The dimensionless ratio of electric conductivity to temperature σ_0/T has been found close to the LQCD results for $N_f = 2 + 1$. In the vicinity of T_c we find a good agreement between the DQPM results and the predictions from the Chapman-Enskog approximation for massless quarks and gluons. The ratio σ_0/T shows slight increase in μ_B similar to the viscosities. Since there are no available LQCD calculations of κ_B , it is interesting to estimate κ_B and its μ_B -dependence. Actual DQPM results for the dimensionless ratio of the baryon diffusion coefficient to the temperature squared κ_B^{RTA}/T^2 are in agreement with the estimates from the Chapman-Enskog approximation for massless quarks and gluons near T_c . Moreover, we have estimated the value of κ_B^{SS}/T^2 as suggested by the AdS/CFT approach using the DQPM equation of state, taking into account the KSS bound for the shear viscosity to entropy density ratio. The actual values for κ_B^{RTA}/T^2 are larger than κ_B^{SS}/T^2 for all considered μ_B values.

In conclusion, we have found only a very weak dependence on μ_B for all transport coefficients considered in this study. The shear and bulk viscosities, electric

conductivities of the quark-gluon plasma increase with increasing μ_B while the diffusion baryon coefficient decreases. This is interesting in light of a recent finding that the baryon diffusion might enhance the difference between proton and antiproton elliptic flow $v_2(p_T)$ and mean transverse momenta.

ACKNOWLEDGMENTS

The authors acknowledge inspiring discussions with W. Cassing, J. M. Torres-Rincon, J. Aichelin, H. Berrehrah, C. Ratti, E. Seifert, A. Palmese and T. Steinert. Fur-

thermore, we would like to thank J. A. Fotakis for sharing Chapman-Enskog results for the baryon diffusion coefficient and the electric conductivity. This work was supported by the LOEWE center "HIC for FAIR". Furthermore, P.M., and E.B. acknowledge support by the Deutsche Forschungsgemeinschaft (DFG, German Research Foundation) through the grant CRC-TR 211 'Strong-interaction matter under extreme conditions' - Project number 315477589 - TRR 211. O.S. acknowledges support from HGS-HiRe for FAIR; E.B. thanks the COST Action THOR, CA15213. The computational resources have been provided by the LOEWE-Center for Scientific Computing.

-
- [1] L. Adamczyk et al. (STAR), Phys. Rev. C **96**, 044904 (2017), arXiv:1701.07065 [nucl-ex].
 - [2] T. Ablyazimov et al. (CBM), Eur. Phys. J. A **53**, 60 (2017), arXiv:1607.01487 [nucl-ex].
 - [3] A. N. Sissakian and A. S. Sorin (NICA), Strangeness in quark matter. Proceedings, International Conference, SQM 2008, Beijing, P.R. China, October 5-10, 2008, J. Phys. G **36**, 064069 (2009).
 - [4] W. Cassing, Eur. Phys. J. ST **168**, 3 (2009); Nucl. Phys. A **795**, 70 (2007).
 - [5] B. Vanderheyden and G. Baym, J. Stat. Phys. **93**, 843 (1998).
 - [6] J. P. Blaizot, E. Iancu and A. Rebhan, Phys. Rev. D **63**, 065003 (2001).
 - [7] C. Sasaki and K. Redlich, Phys. Rev. C **79**, 055207 (2009).
 - [8] M. Bluhm, B. Kämpfer, and K. Redlich, Phys. Rev. C **84**, 025201 (2011).
 - [9] R. Marty, E. Bratkovskaya, W. Cassing, J. Aichelin, H. Berrehrah, Phys. Rev. C **88**, 045204 (2013).
 - [10] P. Moreau, O. Soloveva, L. Oliva, T. Song, W. Cassing, and E. Bratkovskaya, Phys. Rev. C **100**, 014911 (2019).
 - [11] V. Mykhaylova, M. Bluhm, K. Redlich, and C. Sasaki, Phys. Rev. D **100**, 034002 (2019).
 - [12] O. Linnyk, E. L. Bratkovskaya, and W. Cassing, Prog. Part. Nucl. Phys. **87**, 50 (2016).
 - [13] H. Berrehrah, W. Cassing, E. Bratkovskaya, and T. Steinert, Phys. Rev. C **93**, 044914 (2016).
 - [14] H. Berrehrah, E. Bratkovskaya, T. Steinert, and W. Cassing, Int. J. Mod. Phys. E **25**, 1642003 (2016).
 - [15] S. Borsanyi, Z. Fodor, C. Hoelbling, S. D. Katz, S. Krieg and K. K. Szabo, Phys. Lett. B **730**, 99 (2014).
 - [16] S. Borsanyi, G. Endrödi, Z. Fodor, S. D. Katz, S. Krieg, C. Ratti and K. K. Szabo, JHEP **1208**, 053 (2012).
 - [17] T. Steinert and W. Cassing, J. Phys. Conf. Ser. **1024**, 012029 (2018).
 - [18] J. Cleymans, H. Oeschler, K. Redlich, and S. Wheaton, Phys. Rev. C **73**, 034905 (2006).
 - [19] A. Palmese, W. Cassing, E. Seifert, T. Steinert, P. Moreau, and E. L. Bratkovskaya, Phys. Rev. C **94**, 044912 (2016).
 - [20] A. Hosoya and K. Kajantie, Nucl. Phys. B **250**, 666 (1985).
 - [21] R. Kubo, J. Phys. Soc. Jpn. **12**, 570 (1957).
 - [22] G. Aarts and J. M. Martinez Resco, J. High Energy Phys. **04**, 053 (2002).
 - [23] P. Chakraborty and J. I. Kapusta, Phys. Rev. C **83**, 014906 (2011).
 - [24] M. Albright and J. I. Kapusta, Phys. Rev. C **93**, 014903 (2016).
 - [25] S. Gavin, Nucl. Phys. A **435**, 826 (1985).
 - [26] D. F. Fraile, A. G. Nicola, Phys. Rev. D **73**, 045025 (2006).
 - [27] R. Lang, N. Kaiser, and W. Weise, Eur. Phys. J. A **48**, 109 (2012).
 - [28] V. Ozvenchuk, O. Linnyk, M. I. Gorenstein, E. L. Bratkovskaya, and W. Cassing, Phys. Rev. C **87**, 064903 (2013).
 - [29] E. Shuryak, Prog. Part. Nucl. Phys. **53**, 273 (2004).
 - [30] M. Gyulassy and L. McLerran, Nucl. Phys. A **750**, 30 (2005).
 - [31] U. W. Heinz, arXiv:nucl-th/0512051.
 - [32] N. Astrakhantsev, V. Braguta, and A. Kotov, J. High Energy Phys. **04**, 101 (2017).
 - [33] S. A. Bass, J. E. Bernhard and J. S. Moreland, Nucl. Phys. A **967**, 67 (2017).
 - [34] S. Ryu, J. - F. Paquet, C. Shen, G. S. Denicol, B. Schenke, S. Jeon, and C. Gale, Phys. Rev. Lett. **115**, 132301 (2015).
 - [35] N. Yu. Astrakhantsev, V.V. Braguta, and A. Yu. Kotov, Phys. Rev. D **98** no.5, 054515 (2018).
 - [36] H. B. Meyer, Phys. Rev. Lett. **100**, 162001 (2008).
 - [37] Y. Xu, P. Moreau, T. Song, M. Nahrgang, S. A. Bass, and E. Bratkovskaya, Phys. Rev. C **96**, no. 2, 024902 (2017).
 - [38] T. Steinert and W. Cassing, Phys. Rev. C **89**, no. 3, 035203 (2014).
 - [39] W. Cassing, O. Linnyk, T. Steinert, and V. Ozvenchuk, Phys. Rev. Lett. **110**, no. 18, 182301 (2013).
 - [40] Y. Yin, Phys. Rev. C **90**, 044903 (2014).
 - [41] S. Turbide, R. Rapp, and C. Gale, Phys. Rev. C **69**, 014903 (2004).
 - [42] O. Linnyk, W. Cassing, and E. Bratkovskaya, Phys. Rev. C **89**, (2013).
 - [43] Y. Akamatsu, H. Hamagaki, T. Hatsuda, and T. Hirano, J. Phys. G **38**, 124184 (2011).
 - [44] A. Puglisi, S. Plumari, and V. Greco, Phys. Rev. D **90**, 114009 (2014).
 - [45] L. Thakur, P. K. Srivastava, G. P. Kadam, M. George, and H. Mishra, Phys. Rev. D **95**, 096009 (2017).

- [46] B. B. Brandt, A. Francis, H. B. Meyer, and H. Wittig, JHEP **1303**, 100 (2013).
- [47] B. B. Brandt, A. Francis, H. B. Meyer, and H. Wittig, PoS ConfinementX, 186 (2012).
- [48] B. B. Brandt, A. Francis, B. Jäger, and H. B. Meyer, Phys. Rev. D **93**, no. 5, 054510 (2016).
- [49] A. Amato, G. Aarts, C. Allton, P. Giudice, S. Hands, and J. I. Skullerud, Phys. Rev. Lett. **111**, no. 17, 172001 (2013).
- [50] G. Aarts, C. Allton, A. Amato, P. Giudice, S. Hands, and J. I. Skullerud, JHEP **1502**, 186 (2015).
- [51] M. Greif, J. A. Fotakis, G. S. Denicol, and C. Greiner, Phys. Rev. Lett. **120**, 242301 (2018).
- [52] P. K. Kovtun, D. T. Son, and A. O. Starinets, Phys. Rev. Lett. **94**, 111601 (2005).
- [53] R. Rougemont, R. Critelli, J. Noronha-Hostler, J. Noronha, and C. Ratti, Phys.Rev. D **96** no.1, 014032 (2017).
- [54] P. Moreau, O. Linnyk, W. Cassing, and E. Bratkovskaya, Phys. Rev. C **93**, 044916 (2016).
- [55] V. Ozvenchuk, O. Linnyk, M. I. Gorenstein, E. L. Bratkovskaya, and W. Cassing, Phys. Rev. C **87**, 024901 (2013).
- [56] D. T. Son and A. O. Starinets, J. High Energy Phys. **0603**, 052 (2006).
- [57] A. Jaiswal, B. Friman, and K. Redlich, Phys. Lett. B **751**, 548-552 (2015).
- [58] G. S. Denicol, C. Gale, S. Jeon, A. Monnai, B. Schenke, and C. Shen, Phys. Rev. C **98**, 034916 (2018).